Raman and CD Spectroscopy of Recombinant 68-kDa DNA Human Topoisomerase I and Its Complex with Suicide DNA−Substrate†

Fabrice Fleury,§ Anatoli Ianoul,§,‖ Eugene Kryukov,‖ Alyona Sukhanova,‖ Irina Kudelina,‖ Abigai Wynne-Jones,⊥ Igor B. Bronstein,⊥,⊗ Michaël Maizieres,§ Maurice Berjot,§ Guy G. Dodson,⊥ Anthony J. Wilkinson,⊥ Joseph A. Holden,○ Alexei V. Feofanov,‖ Alain J. P. Alix,§ Jean-Claude Jardillier,§ and Igor Nabiev*,§

Institut Fédératif de Recherche "Biomolécules", Université de Reims Champagne-Ardenne, 51096 Reims Cedex, France, Optical Spectroscopy Division, Shemyakin & Ovchinnikov Institute of Bioorganic Chemistry, Russian Academy of Sciences, 117871 Moscow, Russia, Department of Chemistry and Yorkshire Cancer Research, University of York, York, YO1 5DD, U.K., and Department of Pathology, University of Utah Health Sciences Center, Salt Lake City, Utah, 84132

Received March 20, 1998; Revised Manuscript Received July 16, 1998

ABSTRACT: N-terminally truncated recombinant 68-kDa human topoisomerase (topo) I exhibits the same DNA-driving activities as the wild-type protein. In the present study, Raman and circular dichroism techniques were employed for detailed structural characterization of the 68-kDa human topo I and its transformations induced by the suicide sequence-specific oligonucleotide (solig) binding and cleavage. Spectroscopic data combined with statistical prediction techniques were employed to construct a model of the secondary structure distribution along the primary protein structure in solution. The 68-kDa topo I was found to consist of ca. 59% α-helix, 24% β-strand and/or sheets, and 17% other structures. A secondary structure transition of the 68-kDa topo I was found to accompany solig binding and cleavage. Nearly 15% of the α-helix of 68-kDa topo I is transferred within the other structures when in the complex with its DNA substrate. Raman spectroscopy analysis also shows redistribution of the structural rotamers of the 68-kDa topo I disulfide bonds and significant changes in the H-bonding of the Tyr residues and in the microenvironment/conformation of the Trp side chains. No structural modifications of the DNA substrate were detected by spectroscopic techniques. The data presented provide the first direct experimental evidence of the human topo I conformational transition after the cleavage step in the reaction of binding and cleavage of DNA substrate by the enzyme. This evidence supports the model of the enzyme function requiring the protein conformational transition. The most probable location of the enzyme transformations was the core and the C-terminal conservative 68-kDa topo I structural domains. By contrast, the linker domain was found to have an extremely low potential for solig-induced structural transformations. The pattern of redistribution of protein secondary structures induced by solig binding and covalent suicide complex formation supports the model of an intramolecular bipartite mode of topo I/DNA interaction in the substrate binding and cleavage reaction.

The reaction of eukaryotic topoisomerase (topo[1]) I-induced DNA relaxation involves (i) DNA recognition and binding, (ii) DNA cleavage, during which topo I is covalently attached to the 3′-side of the single-stranded nick, (iii) swiveling of the single DNA strand, (iv) DNA religation, and (v) re-adoption of an initial enzyme conformation (*1*). DNA cleavage is the most thoroughly studied of these steps. The human topo I cleavage sites obey consensus sequences of 10−16 bases (*1*, *2*).

It was recently shown (*3*) that native human (91 kDa) topo I can be divided into four major domains on the basis of sequence analysis and functional mapping: a sparsely conserved N-terminal domain (24 kDa), a conserved core domain (54 kDa), a poorly conserved linker region (5 kDa), and the highly conserved COOH-terminal domain (8 kDa), which contains the active site tyrosine-723. A ∼70-kDa N-terminally truncated fragment and its sensitivity to inhibition by camptothecin (CPT) and metal ions are indistinguishable from those of the intact enzyme based on its sensitivity to CPT and activity by metal ions (*4*).

Very recently, the structures of the covalent and noncovalent complexes of the "reconstituted" human topo I fragment missing N-terminal and linker domains and of the noncovalent complex of the N-terminally truncated nonactive 70-kDa topo I mutant with the suicide DNA substrates have been solved (*5*, *6*). Nevertheless, the data may not provide

† This research was supported by the Association pour la Recherche Contre le Cancer (France, Grant 1379), Russian Foundation for Basic Research, Yorkshire Cancer Research, and in part, by a grant from ARERS (France). A.F. was supported by an FRM fellowship.

* Author to whom correspondence should be addressed at UPRES EA2063, Institut Fédératif de Recherche "Biomolécules" UFR de Pharmacie, Université de Reims Champagne-Ardenne, 51 rue Cognacq Jay, 51096 Reims Cedex, France. E-mail: igor@hexanet.fr.

§ Université de Reims Champagne-Ardenne.

‖ Russian Academy of Sciences.

⊥ Department of Chemistry, University of York.

⊗ Yorkshire Cancer Research, University of York.

○ University of Utah.

[1] Abbreviations: topo I, human DNA topoisomerase I; 68-kDa topo I, recombinant human 68-kDa DNA topoisomerase I; CPT, camptothecin; CD, circular dichroism; solig, suicide sequence-specific oligonucleotide; sc, supercoiled.

S0006-2960(98)00649-7 CCC: $15.00
Published on Web 09/19/1998

an insight on the structural modifications of the enzyme induced by the substrate binding because these successful structural studies were restricted to the topo I/DNA complexes. The crystals of the free enzyme were not obtained, and there is no information concerning the structure of free topo I.

Mechanistic studies of the topo I cleavage reaction are difficult because a topo I/DNA covalent intermediate is very transient. Nevertheless, studies of the eukaryotic topo I mediated cleavage and rejoining reactions are particularly important, since many anticancer drugs act by stabilizing the topo I/DNA covalent intermediates (reviewed in ref *7*).

To provide the means for uncoupling the DNA cleavage and religation steps, extensive studies of various DNA substrates for trapping the covalent enzyme/DNA intermediates have been performed. It was found (*8*) that these topo I mediated half reactions may be uncoupled with highly efficient, site-specific, so-called "suicide" DNA substrates. These substrates contain nicks near the site of cleavage so that a small incised fragment is released following strand cleavage, thereby removing the critical 5′-OH necessary for strand ligation (*2*, *8*).

Here, we present a comparative structural characterization of recombinant human 68-kDa topo I (an enzyme starting from lysine-191 of the sequence of the full-length protein and exhibiting all DNA-driving properties of the full-length protein) and 68-kDa topo I/DNA complex using spectroscopic Raman and CD techniques and predictional theoretical approaches (*9*, *10*). The methods of LINK (*10*, *11*) close the gap between empirical prediction of protein conformation and optical spectroscopy data. It has been used to adjust the set of local secondary structure predictions by taking into account the experimental estimation of the global secondary structures.

In this study, suicide sequence-specific oligonucleotide (solig) was used to uncouple 68-kDa topo I cleavage and religation reactions to examine 68-kDa topo I conformational transitions induced by solig binding and cleavage. Considerable secondary structure transition, changes in the configuration of the disulfide bonds, strong variations of the H-bonding state of the Tyr residues, and changes in the environment and orientation of the side chains of Trp residues of the 68-kDa human topo I were found to accompany solig binding and cleavage by the enzyme. These data provide the first experimental proof of significant conformational transition in the course of the 68-kDa human topo I/DNA binding and cleavage reaction. Spectroscopic data concerning the structure of topo I and topo I/DNA complexes in solution are compared with the recently published structures of topo I/DNA covalent and noncovalent complexes in crystals (*5*, *6*).

MATERIALS AND METHODS

Enzymes and Chemicals. Restriction enzymes, Klenow fragment, T4 DNA ligase, and T4-polynucleotide kinase were purchased from Promega or New England Biolabs. [γ-^{32}P] ATP was from Amersham. Affinity purified goat antimouse horseradish peroxidase conjugate was from Bio-Rad. N-terminal protein sequencing was carried out in the Centre for Mechanisms of Human Toxicity, University of Leicester, UK. Other chemicals were purchased as follows: PMSF, individual protease inhibitors, MES, CAPS, imidazole, and CPT from Sigma; Tris and protease inhibitors cocktail tablets from Boehringer Mannheim; PEG-6000 from the BDH.

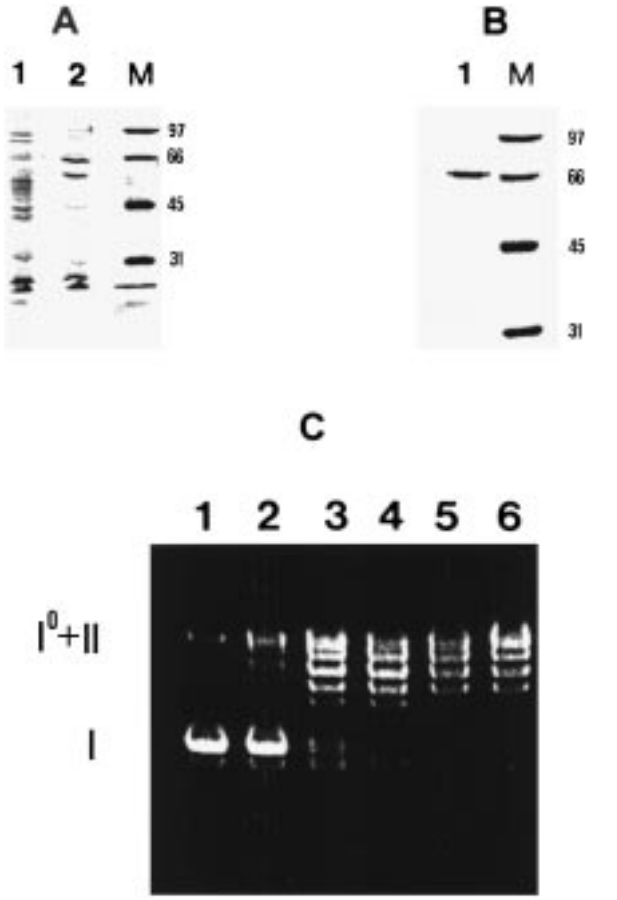

FIGURE 1: Expression, purification, and characterization of human 68-kDa topo I from insect cells. Coomassie blue stained 8.75% denaturing polyacrylamide gels run under reducing conditions, showing the induction of expression (A) and the purification of 68-kDa topo I (B, C). (A) Lane 1: 2 μL of the PEG-6000 supernatant, corresponding to 40 μL of uninduced insect cell suspension. Lane 2: the same amount of PEG-6000 supernatant from a virally infected insect cell suspension. Lane M: markers (Bio-Rad) whose molecular masses in kilodaltons are indicated. (B) 1 μg of pure 68-kDa topo I after chromatography on the Pharmacia Resource S10 column. Lane M: molecular size markers. (C) Time course of the relaxation of supercoiled DNA catalyzed by 68-kDa topo I. An amount of 20 ng of purified 68-kDa topo I was added to a 10 μL reaction mix containing 1 μg of sc pGEM7Z DNA. Topoisomers were resolved by electrophoresis in a 1% agarose gel. Lane 1: untreated DNA. Lanes 2−6: treatment of sc pGEM7Z with 68-kDa topo I for 0.5, 1, 2, 5, and 10 min, respectively. The positions of sc pGEM7Z (I) and fully relaxed and nicked DNA ($I^0 + II$) are indicated. A ladder of partially relaxed DNA appears following incubation with topo I.

Recombinant 68-kDa Human Topo I. The detailed protocol for construction of plasmids, containing genes of N-terminally truncated 68-kDa human topo I, enzyme expression in the insect cells, and protein purification will be published elsewhere.

Recombinant baculoviruses were engineered to express a truncated topo I beginning at Lys-191. After infection of *S. frugiperda* with these viruses, 68-kDa topo I is efficiently expressed, reaching peak levels after 72 h. This protein can be purified to homogeneity in a simple two-column procedure, yielding 5−10 mg of pure 68-kDa topo I per liter of culture (Figure 1).

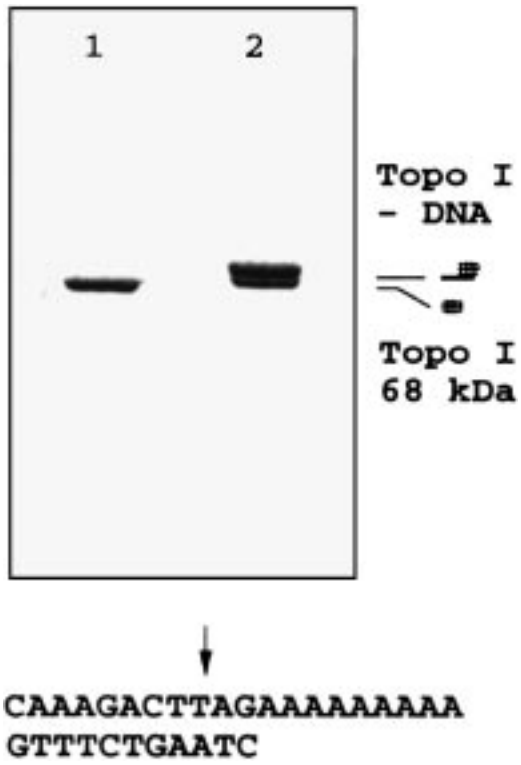

FIGURE 2: 68-kDa topo I cleavage of solig. The 68-kDa topo I was incubated for 30 min at 22 °C in the presence or absence of a large excess of the solig prior to the addition of SDS, to trap the cleavable complexes, analysis of the products by 8.75% denaturing polyacrylamide gel electrophoresis, and staining with Coomassie blue. Lane 1: free 68-kDa topo I. Lane 2: 68-kDa topo I incubated with solig.

Oligonucleotides. Synthetic oligonucleotides were synthesized on a DNA synthesizer model 392 from Applied Biosystems according to protocol specified by the manufacturer. Oligonucleotides were purified by polyacrylamide gel electrophoresis [(12−18% polyacrylamide (19:1)−8 M urea, 0.5× TBE (44 mM Tris, 44 mM boric acid, 1 mM Na_2−EDTA)], electroeluted (Schleicher and Schuell Elutrap) in 0.5× TBE, concentrated by lyophilization, and desalted over a Bio-Gel P6 (BioRad) spin column.

The following sequence-specific suicide oligonucleotide was used as the topo I substrate in this study: 5′-CTAAGTCTTTG-3′; 5′-CAAAGACTTAGAAAAAAAAA-3′.

Preparation of DNA/Protein Complexes. Olig was labeled at the 5′-end prior to annealing using T4 polynucleotide kinase and [γ-^{32}P] ATP. The labeled olig was annealed to a complementary unlabeled olig and duplex DNA was gel-purified. Purified topo I in the amount of 5 pmol was incubated with 2 pmol of 18 mer duplex DNA (5′-end labeled either on the scissile or nonscissile DNA strand) in 20 μL of 30 mM potassium phosphate buffer pH 7.2 for 30 min at 37 °C.

Alternatively, the complex can be observed through the altered mobility of the protein in SDS−PAGE. For these experiments, 5−30 pmol of the topo I fragment was incubated in the presence of 200 pmol of unlabeled DNA.

DNA-Cleavage Activity of Recombinant 68-kDa Topo I. The 68-kDa topo I/DNA cleavage reactions were carried out using solig substrate, which contains a consensus cleavage sequence for topo I (Figure 2). The products of the reaction between 68-kDa topo I and the DNA substrate were visualized using SDS−PAGE gel electrophoresis. A cleavable complex was formed after incubation of 68-kDa topo I with solig duplex (Figure 2), a highly unstable partial duplex downstream of this site that is held together by only two bp. As a result, the downstream segment of the cleaved top strand freely diffuses from the complex trapping the enzyme in a covalent complex with DNA. The yield of enzyme/DNA covalent complex was insensitive to pH in the range 6−8 and temperature in the range 25−37 °C; however, increasing concentrations of NaCl substantially lowered the amount of this complex.

FLD Spectroscopy. The FLD spectra were measured as a function of time using a JASCO-500C dichrograph equipped with an Oxley prism. Supercoiled (sc) plasmid DNA was oriented by the flow gradient provided by pumping the solution through the flow cell as described (*12*). The cell volume was 200 μL with an optical path length of 2 mm and a flow gradient in the cell of 6000 s^{-1}. The linear dichroism signal was found to increase continuously with the flow gradient, and no artifacts due to turbulent flow were observed. Experiments were performed in a reaction mixture containing 20 mM Tris HCl, pH 7.5, 100 mM NaCl, 5% (v/v) glycerol, 0.05 mg/mL BSA, 0.5 mM EDTA, and 3 μg of pUC19 plasmid. CPT stock solution was made in DMSO at a concentration of 0.1 mM. Corresponding amounts of drugs were added to the reaction mixture containing sc plasmid immediately before the FLD experiment.

Biochemical and Flow Linear Dichroism DNA Relaxation Assay. We have combined agarose gel-electrophoretic methods and the recently developed FLD technique to monitor the relaxation of pUC19 plasmid DNA by 68-kDa topo I. DNA relaxation by topo I reduces the linking number of sc DNA in steps of one and thereby alters its hydrodynamic properties. The electrophoretic mobility of DNA in agarose gels is sensitive to the linking number, and this has become the standard method for monitoring topo's reactions. FLD has the advantage of continuous monitoring of this process in a real time. It monitors the degree of orientation of the DNA in the flow apparatus, which is manifested as a difference in absorbance of light polarized in orthogonal directions (*12*).

The electrophoretic assay was performed with 0.5 μg of negatively sc plasmid DNA treated with topo I or soluble protein extract in 20 μL of 50 mM Tris-HCl pH 7.5, 0.1 M NaCl at 25 °C for 5 min. The reactions were stopped by addition of 0.5% SDS and analyzed by electrophoresis in a 0.8−1.0% agarose gel run in TBE buffer.

Figure 3 shows time courses of the change in the FLD signal following mixing of 68-kDa topo I with sc DNA in the presence and absence of different concentrations of CPT. In the absence of the drug, there is a hyperbolic rise in the ΔA_{rel} associated with the relaxation of the DNA. The assay demonstrate that 68-kDa topo I has an efficient relaxation activity practically identical to that of the full-length enzyme. These reactions are inhibited by CPT at concentrations similar to those which inhibit the intact enzyme. The inhibition of the enzyme correlates well with the electrophoresis data performed at identical conditions (Figure 3).

Circular Dichroism (CD) and Raman Spectroscopy. Samples of 68-kDa topo I for CD and Raman spectroscopy were concentrated by microfiltration to 9 mg/mL in 20 mM potassium phosphate buffer (pH 7.5), 150 mM NaCl. No

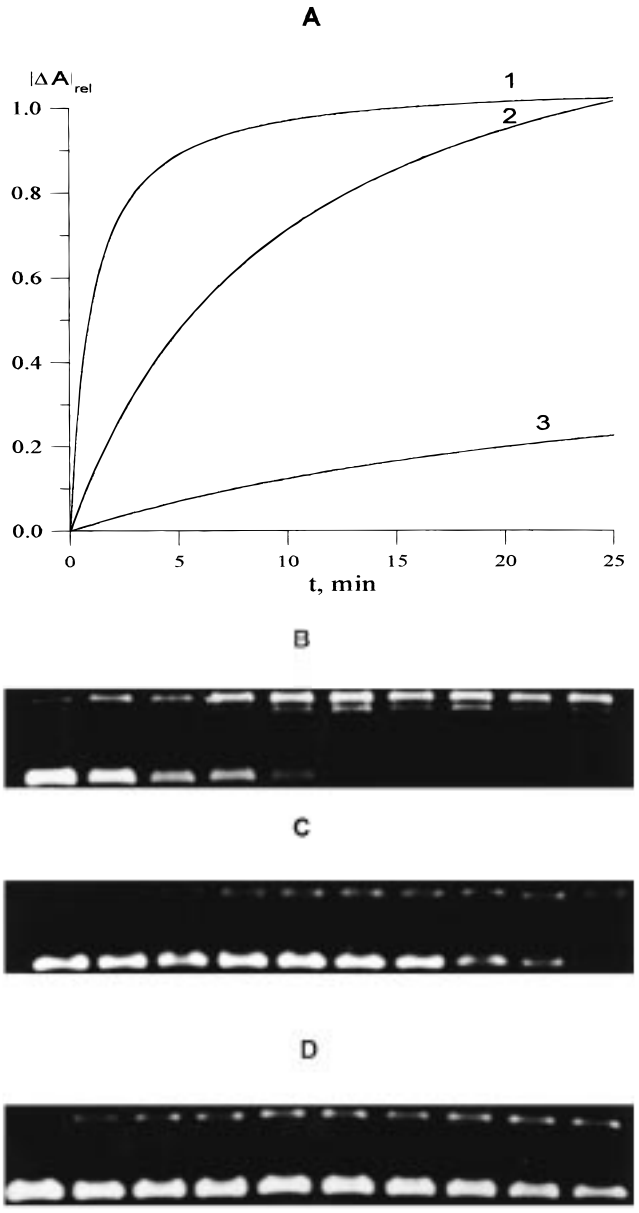

FIGURE 3: Kinetics of 68-kDa topo I catalyzed relaxation of sc DNA monitored by FLD (A) and agarose electrophoresis (B−D). Sc pUC19 DNA [36 μM] was incubated with 68-kDa topo I [12 nM] in the presence of 0 (curve 1 and part B), 1 μM (curve 2 and part C) and 10 μM (curve 3 and part D) CPT. The electrophoresis and the measurements of FLD signal were performed at 20 °C.

evidence of formation of the protein aggregates was found at this concentration and ionic strength. The samples were centrifuged for 5 min at 400*g*, and the aliquots were transferred into a 0.001 cm CD quartz cell or into a 3 mm Raman quartz cell. The complex of 68-kDa topo I with solig was prepared by diluting lyophilized solig in a solution of 68-kDa topo I to obtain a 68-kDa topo I/solig in a 1:1 molar ratio.

CD spectra were measured with a Jasco-500C (Jasco, Japan) dichrograph in the region 350−185 nm with a time constant of 1 or 2 s. The CD spectra were scaled to molecular ellipticity ($\Delta\epsilon$). To calculate the secondary structure of the enzyme in complex with solig, the CD spectrum of solig in water was subtracted from the spectrum of the 68-kDa topo I/solig complex, using the 280 nm band of solig for normalization. Such a normalization of spectra is valid, since the 280 nm band is characteristic of B-DNA, and its intensity is the same for both the 68-kDa topo I/solig complex and pure solig.

Raman spectra were recorded in the region 400−1800 cm^{-1} with a scanning increment of 1 cm^{-1} and an integration time of 5 s using a Ramanor HG-2S (Jobin Yvon, France) spectrometer. The spectra were collected as an average of 40 scans. A 514.5 nm line of the Ar-ion laser (Spectra Physics, model 164-03, USA), operating with 400 mW of power at the sample, was used for excitation. The Raman spectrum of the buffer was recorded exactly in the same conditions and subtracted from the spectrum of 68-kDa topo I. Stability of the protein during the Raman spectrum acquisition was controlled by comparison of consequent scans and CD spectra of specimens before and after Raman experiments. All spectra were reproduced 3 times for different preparations of sample.

The spectra of the protein were subjected to curve deconvolution, using the Spectra Calc software package. For deconvolution purposes, the Raman signal of solig was subtracted from the spectrum of the 68-kDa topo I/solig complex using the 1093 cm^{-1} band of the phosphate backbone vibration of solig as an internal intensity standard. This band is nearly constant in intensity for B-DNA over a wide range of ionic strengths and temperatures and is known to be a sufficient internal intensity standard for DNA/protein complexes (*13*).

Calculation of Protein Conformation from CD and Raman Spectra. The secondary structure of free 68-kDa topo I and that of topo I in complex with solig were calculated from CD spectra using a CONTIN-LG (LG3) version of the original CONTIN- program (*14*). The secondary structure of the enzyme was calculated from Raman spectra using the 1630−1700 cm^{-1} region of the amide I mode as described (*15*−*17*). The reference intensity profiles (RIP) method (*18*) rather than the partial least-squares (PLS) regression (*19*) and principle component regression (PCR) techniques (*20*) was chosen for the calculations because, as applied to the reference set of 15 proteins, it gives correlation coefficients (X-ray versus Raman data) higher than 0.97 for each class of structure, with the average error being below 2% (*15*). Using the RIP technique, the relative contributions of the reference profiles corresponding to α-helix, β-sheet, and other secondary structures are calculated together with the solvent profile in the amide I region. As a result, an optimal subtraction coefficient for solvent profile contribution may be determined after optimization of the amide I band decomposition procedure that significantly improves the results of calculations.

Statistical Predictions of Secondary Structure. The strategy of our secondary structure prediction from the amino acid sequence of 68-kDa topo I was as follows. Starting with the protein sequence, the most probable α-helix and β-sheet segments were predicted using the Chou−Fasman (*21*) and GOR-1 methods (*22*), and the labile fragments, which may adopt any conformation with equal probability, were identified. Then, we used the LINK methods (*10*, *11*) to adjust the data of prediction methods by taking into account the Raman experimental data on the protein conformation and data on protein class structure.

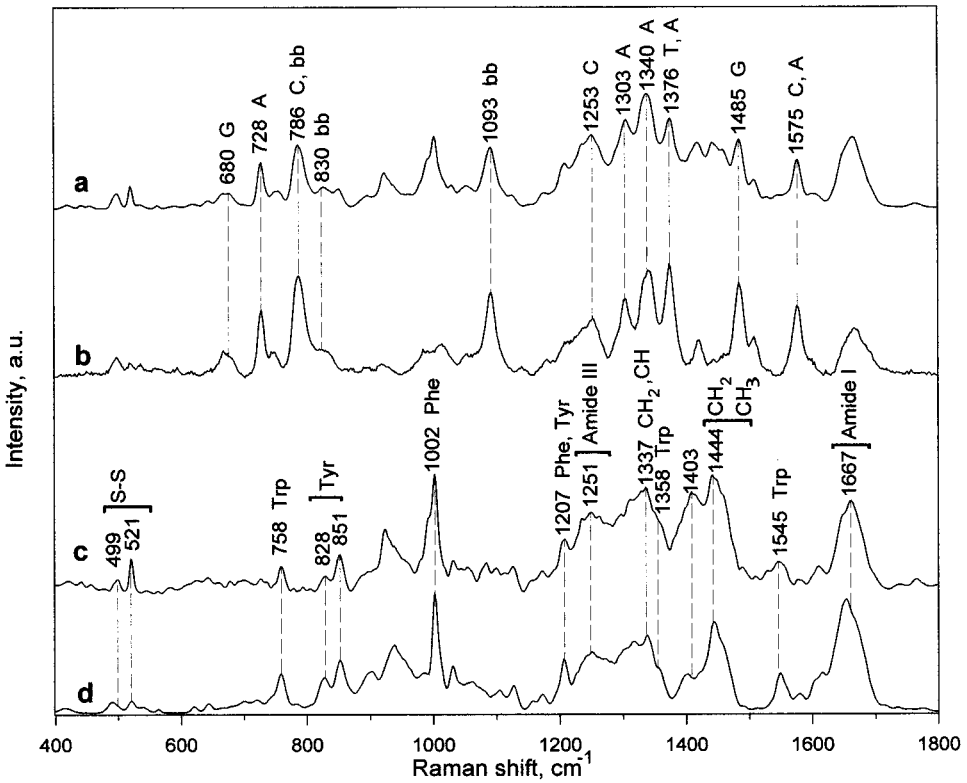

FIGURE 4: Raman spectra of 68-kDa topo I/solig complex (a), solig (b), topo/solig with subtracted solig (c), and free 68-kDa topo I (d). The 68-kDa topo I concentration is ca. 9 mg/mL. Molar ratio 68-kDa topo I/solig is 1:1. Other experimental conditions are given in the text.

RESULTS

We choose to express the enzyme as an N-terminally truncated form for the following reasons. First, topo I proteolytic fragments are commonly reported in preparations of the enzyme from a variety of sources and create problems in purification and handling. The observations with the topo I proteins expressed in yeast show that proteolysis is taking place at the N-terminus. Second, it has been known for many years that a 65−70-kDa fragment of topo I retains all of the DNA driving activities of the intact enzyme and being isolated from many mammalian tissues was shown to be very stable. We therefore purified this 65−70-kDa fragment from human placental tissue and performed cycles of Edman degradation to establish its N-terminus. Seven such cycles gave the sequence Lys-Lys-Lys-Lys-Pro-Lys-Lys, indicating that the fragment starts at Lys-191. If the C-terminus of the protein is intact, this molecule has a predicted molecular mass of 68 kDa.

Recombinant human 68-kDa topo I purified according to our procedure is active in DNA cleavage and relaxation (Figures 1 and 3) and forms the covalent complex in a similar manner as that described for the intact topo I purified from yeast (Figure 2). Overall, 68-kDa topo I displays very similar cleavage specificity and sensitivity to CPT to the full-length topo I.

68-kDa Topo I and Its Complex with Solig: Comparative Raman Analysis. The Raman spectrum of a 9 mg/mL standard buffered solution of 68-kDa topo I and the Raman spectrum of the 68-kDa topo I/solig complex in the region 400−1800 cm^{-1} are shown in Figure 4. The spectra have no significant fluorescence contribution in the visible region. The excellent signal-to-noise ratio achieved enables us to make a practically total spectral decomposition of all of the individual Raman bands so that the theoretical spectrum reconstituted from the individual band components shows less than a 2% difference from the experimental spectrum. This result makes possible a detailed quantitative analysis of the bands in the Raman spectrum of 68-kDa topo I.

All prominent Raman bands in the spectrum of the 68-kDa topo I are assigned to protein groups as indicated in Figure 4c. In the following analysis, we make use of well-established Raman spectra−structure correlation (*23*) to determine side-chain characteristics and secondary structures. In general, the bands in the Raman spectrum are sensitive in frequency and intensity to the conformation and environment of the molecular groups. Key bands of interest are those of amide I and amide III, which have their origins in vibrations of the protein main chain and provide characteristics of the secondary structure (*23*). On the other hand, the bands of tyrosine, tryptophan, and cysteine residues furnish information on side-chain conformation, hydrogen bonding, and hydrophobic interactions (*23*−*29*).

There is a strong contribution of the solig bands in the Raman spectrum of the 68-kDa topo I/solig complex (Figure 4). Therefore, to perform a comparative analysis of spectra of the enzyme with and without solig and to identify structural changes in 68-kDa topo I under complexation, the spectrum of the solig should be subtracted from the spectrum of the complex. The spectrum of the solig is presented in Figure 4b. This oligonucleotide adopts the B-form in water, as indicated by the bands at ca. 680 cm^{-1} (G, C2-endo/anti), ca. 786 cm^{-1} (C and backbone), 830 cm^{-1}, and 1093 cm^{-1} (backbone) (*30*, *31*). These bands are also observed in the spectrum of the 68-kDa topo I/solig complex (Figure 4a), indicating that no detectable changes in the secondary structure of the solig occur on complexation with the enzyme.

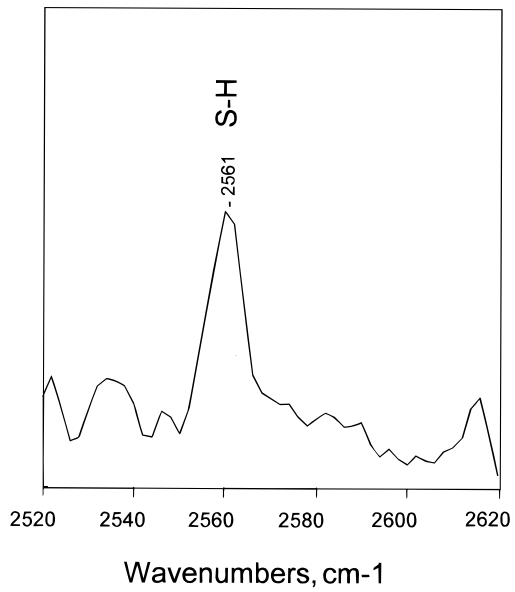

FIGURE 5: Raman spectrum of topo I in the region of S−H vibrations. Experimental conditions are the same as those in Figure 4.

Other markers highly sensitive to DNA conformation include a band near 1376 cm^{-1}, which is sensitive to the pyrimidine C5 methyl group environment, and a band near 1490 cm^{-1} that shifts to 1480 cm^{-1} when guanine N7 accepts a strong hydrogen bond (*32*). In the spectra of solig and the 68-kDa topo I/solig complex, the positions and the intensities of these bands (as well as of the rest modes of the solig) were found to be unchanged. Therefore, the spectrum of the solig can be validly subtracted from the Raman spectrum of the complex. All prominent Raman bands in the spectrum of the bound protein obtained so were assigned to protein groups as indicated in Figure 4.

Side-Chain Vibrations in the Raman Spectra of 68-kDa Topo I. (a) S−H and S−S Regions. There are eight cysteine residues per 68-kDa topo I molecule. Raman spectroscopy provides a unique possibility to detect and analyze the disulfide bonds through the characteristic protein S−S stretching vibrations in the 480−550 cm^{-1} region and, at the same time, allows detection of the bands of SH groups in the 2500−2600 cm^{-1} region (*23*, *29*).

The Raman spectrum of the 68-kDa topo I reveals the band of S−H vibration centered at 2561 cm^{-1} (Figure 5). This band is unusually intense and quite sharp (if compared with Raman spectra of proteins with a single Cys residue) and should correspond to two to four Cys residues per protein molecule (*23*). It was shown that the weak and broad band at ca. 2550 cm^{-1} indicates SH groups involved in hydrogen bonding with strong acceptors (H_2O, C═O, etc.), whereas the sharp and higher frequency band at ca. 2570 cm^{-1} indicates non-hydrogen-bonded or very weakly hydrogen-bonded SH groups, evidently shielded from solvent and other potential H-bond acceptors (*33*, *34*). Quite sharp and intense S−H vibrations in the Raman spectrum of 68-kDa topo I suggest that most of the Cys is buried within the protein environment, and the intermediate (ca. 2561 cm^{-1}) position of this band implies H-bonding to moderate acceptors, such as the NH_2 group of Arg or/and Lys (*29*). Analysis of the pH dependence of the Raman spectrum of 68-kDa topo I is now in progress and should enable us to clarify the state of the individual SH groups within the 68-kDa topo I molecule.

The bands in the 500−540 cm^{-1} region correspond to S−S vibrations of the disulfide bonds with the equilibrium central dihedral angle of the CCS−SCC moiety at ca. 85° (*35*, *36*). The frequencies of the S−S stretching vibrations in this region vary as a function of internal rotation about the C−S bonds of the CC−SS−CC moiety. The vibrations in the region 500−510 cm^{-1} are assigned to a gauche−gauche−gauche (g−g−g) conformation, whereas a gauche−gauche−trans (g−g−t) rotamer(s) gives the band at 515−525 cm^{-1}, and trans−gauche−trans (t−g−t) rotamer(s) reveal themselves at 535−545 cm^{-1} (*35*, *36*). On the other hand, the lower (480−500 cm^{-1}) frequencies of the S−S vibrations correspond to "strained" CCS−SCC dihedral angles and were found to have a linear dependence on the values of the CCS−SCC dihedral angles (*37*, *38*). This means that if the S−S stretching Raman band occurs within the 450−500 cm^{-1} region, it corresponds to a nonequilibrium (far from ca. 85°) value of the CCS−SCC dihedral angle. Moreover, this angle may be calculated from the linear-angle/frequency correlation determined for strained disulfides (*37*, *38*).

Figure 6b shows four decomposed components (489, 498, 521, and 539 cm^{-1}) of the S−S stretching vibrations within the 480−540 cm^{-1} region of the Raman spectrum of the 68-kDa topo I. Two of these bands (489 and 498 cm^{-1}) correspond to the "strained" rotamers, with nonequilibrium values of the CCS−SCC dihedral angles of 18° and 38°, respectively (*37*, *38*). The "strained" conformation of the disulfide bond(s) may not be stable and is most likely affected in protein−substrate interactions and by changes in pH or ionic strength.

Two other S−S bands (Figure 6b) in the region 500−540 cm^{-1} (521 and 539 cm^{-1}) correspond to the g−g−t and t−g−t rotamers of the CC−SS−CC moiety with the equilibrium (ca. 85°) CCS−SCC central dihedral angle. The first rotamer is characterized by the 0−50° and 50−180° CC−SS and SS−CC dihedral angles, respectively. The second should have nearly equal CC−SS and SS−CC dihedral angles in the range 0−50° (*35*, *36*).

Indeed, the four conformational rotamers of the CC−SS−CC group detected in the Raman spectra of the 68-kDa topo I may correspond to various configurations of only one, two, or three disulfide bonds. Significant intensity of the S−S bands in the spectrum of the 68-kDa topo I on comparison to the intensities of the corresponding Raman bands in the spectra of proteins with the known number of disulfide bridges (*23*) leads to the conclusion that there are two or three disulfides per 68-kDa topo I molecule. The choice between these two possibilities is more difficult at this stage. Nevertheless, we should note that the absolute integral intensities of the Raman bands, corresponding to the first two (489 and 498 cm^{-1}) and the second two (521 and 539 cm^{-1}) disulfide rotamers, are practically identical. Moreover, they correspond to exactly 50% of the total integral intensity of all the bands in the region of S−S vibrations. So, it seems reasonable to suggest that there are two disulfide bonds per 68-kDa topo I molecule and each of these bonds may exist in the form of two rotamers. The high intensity of the S−H vibrations in the region 2500−2600 cm^{-1} may be explained in this case by a contribution of as much as four free Cys

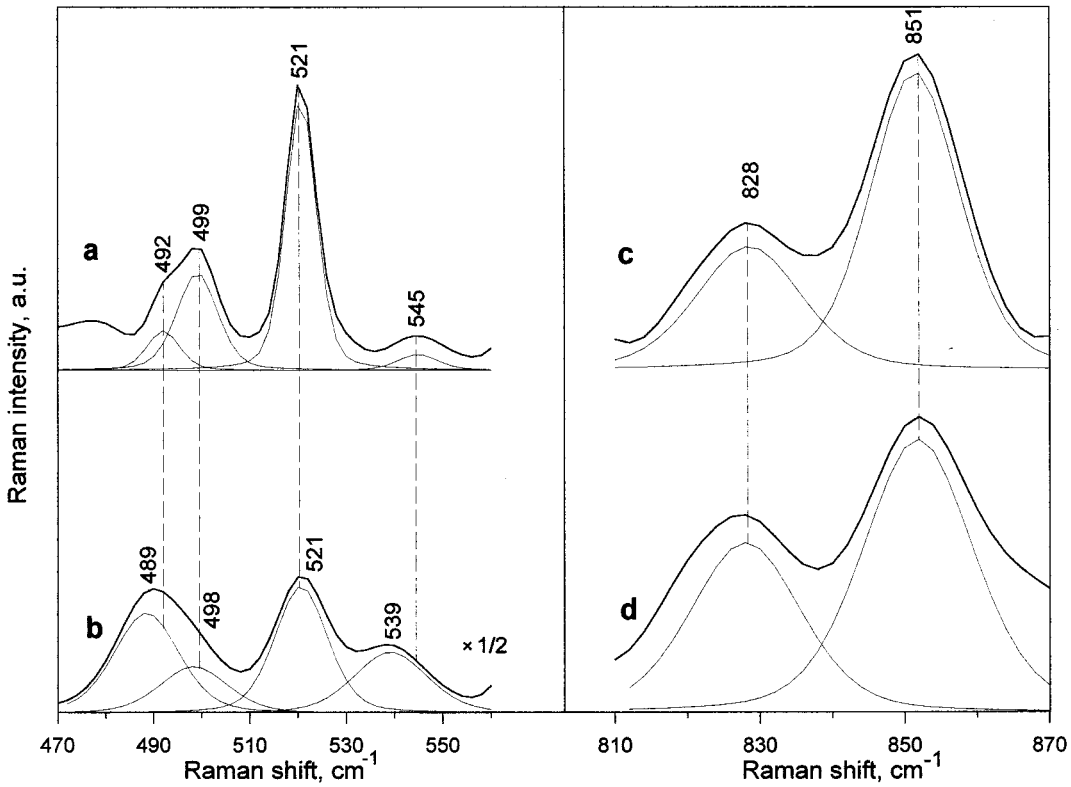

FIGURE 6: Raman spectra in the regions of S−S (a, b) and Tyr (c, d) vibrations for the complex of 68-kDa topo I/solig with subtracted signal of solig (a,c) and for free 68-kDa topo I (b,d).

residues, whereas the four other Cys form two disulfide bonds.

The differential Raman spectrum (68-kDa topo I/solig spectrum minus solig spectrum) also reveals the S−S characteristic features in the 480−550 cm^{-1} region. Figure 6a shows four deconvoluted components (492, 499, 521, and 545 cm^{-1}) of the S−S stretching vibrations in the 480−550 cm^{-1} region of the Raman spectrum of the 68-kDa topo I/solig complex. Two of these bands (492 and 499 cm^{-1}) correspond to the "strained" rotamers with nonequilibrium CCS−SCC dihedral angles of 25° and 39°, respectively (*37*, *38*). The intrinsic instability of the "strained" conformation suggests shifts in the S−S frequencies during protein−substrate interactions. Indeed, the first "strained" rotamer turns out to be affected by interaction with the solig so that the value of the CCS−SCC angle rises from 18° to 25°. Two other S−S bands (521 and 545 cm^{-1}) correspond to the g−g−t and t−g−t rotamers of the CC−SS−CC moiety with the equilibrium (ca. 85°) CCS−SCC central dihedral angle. As for solig-induced changes in the disulfide region, it is important to note that the integral intensities of the Raman bands corresponding to the first two (492 and 499 cm^{-1}) and the second two (521 and 545 cm^{-1}) rotamers always exhibit almost exactly 50% of the total integral intensity of all of the bands in the S−S region. Therefore, the growth of the relative intensity of the "strained" rotamer at 499 cm^{-1} on binding and cleavage of the solig can be suggested to be at the expense of the intensity of the rotamer at 492 cm^{-1}. Similarly, the g−g−t rotamer (521 cm^{-1}) takes its increased intensity from the t−g−t rotamer (545 cm^{-1}). Thus, the solig induces alterations in conformation of the S−S bonds of 68-kDa topo I so that the disulfide moieties display significant perturbations in both the "strained" and t−g−t conformations.

(b) Fermi Resonance Tyrosine Doublet. The well-characterized Fermi resonance doublet of tyrosine (*24*) occurs in 68-kDa topo I at 828 and 851 cm^{-1}, with an unusually high peak intensity ratio of $I_{851}/I_{828} = 1.60$ (Figure 6d). Because there are 19 tyrosine residues per 68-kDa topo I molecule contributing to the observed doublet, no firm conclusions regarding individual tyrosine residues are possible. However, if it is assumed that all tyrosines contribute equally to the doublet intensity, then the present results would be consistent with strong hydrogen bonding of some of the hydroxyl groups as acceptors of H-bonds (*24*). This is the situation expected for tyrosine side chains interacting with proton-donating amino acid side chains (e.g., NH_2 groups of Lys and/or Arg).

One can quantitatively determine the number of buried and exposed tyrosine residues by using the following system of equations (*39*):

$$N_{\text{donor}} + N_{\text{exposed}} + N_{\text{accept}} = 1$$

$$0.5\,N_{\text{donor}} + 1.25\,N_{\text{exposed}} + 2.5\,N_{\text{accept}} = I_{851}/I_{828} \quad (1)$$

where N_{donor}, N_{exposed}, and N_{accept} are the molar fractions of the protein Tyr residues participating in the strong H-bonding as donors of a proton, participating only in the weak H-bonds with the solvent, or participating in the strong H-bond as acceptors of a proton, respectively. The coefficients 0.5, 1.25, and 2.5 are the values of the I_{851}/I_{828} ratio in the Raman spectra of reference proteins with known crystal structures whose tyrosine residues are, respectively, pure strong donors, weak donor/acceptors, or strong acceptors of protons (*24*).

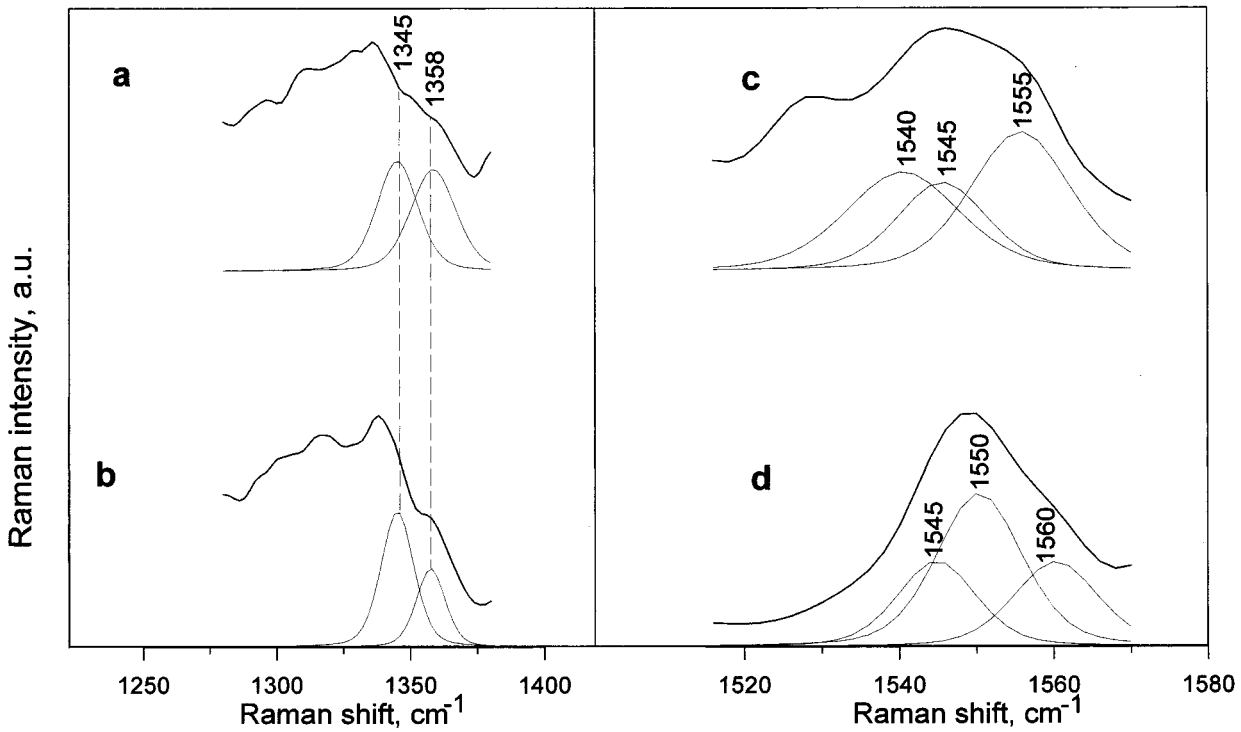

FIGURE 7: Raman spectra of 68-kDa topo I/solig complex (a, c) and of free 68-kDa topo I (b, d) in the regions of Trp vibrations sensitive to microenvironment (a, b) and configuration (c, d) of the side chain. See text for details.

An additional term corresponding to ionized Tyr with the $I_{851}/I_{828} = 0.7$ (*24*) is not included in the system of equations. So far, this ratio has been measured only for the Raman spectra of model compounds. No examples of Raman spectra of ionized tyrosines within the proteins have been reported yet. If the topo I family is concerned, NMR studies of *vaccinia virus* topo I showed that all tyrosines have pK_a values exceeding 9.5 (*40*). That is why the term including contribution of ionized Tyr is neglected for the system of equations describing Tyr residues in the 68-kDa topo I.

The system of equations (1) includes three unknown parameters (N_{accept}, $N_{exposed}$, N_{donor}). Variation of the parameters shows that the system has a solution only if the number of Tyr residues participating in the strong H-bonds as proton acceptors falls in the range 5−10. The number of donors cannot exceed 7 and the number of exposed residues is less than 14.

In complex with the solig, the ratio of I_{851}/I_{828} is even increased to 2.0 (Figure 6c). The same approach was used to estimate the number of residues of each type for the topo I bound to the solig. The results obtained are as follows: the number of acceptors falls in the range 12−15, the number of donors cannot exceed 4, and the number of exposed residues is less than 7. Considering all possible variants of transformations between the two protein states (the 68-kDa topo I alone and its complex with the solig), the number of Tyr residues changing H-bonding state upon complex formation is expected to fall in the range 5−14 with a more probable value of changed residues to be 6.

(c) Tryptophan Residues. There are 13 Trp residues per 68-kDa topo I molecule, and a number of them exist in hydrophobic environments as judged from the characteristic Raman intensity ratio of the bands of Trp at 1358 and 1345 cm^{-1} (*25*). This result is consistent with our fluorescence experiments (data not shown). Unfortunately, the 1345 cm^{-1} band of Trp strongly overlaps with the C-H bending modes, which makes quantitative estimations of Trp in hydrophobic domains based on a I_{1358}/I_{1345} ratio ambiguous (Figure 4). Nevertheless, since the C-H modes are presumed mostly unaffected by molecular surroundings, I_{1358}/I_{1345} can be reliably used to follow the overall changes in the Trp environment (*25*, *41*). This ratio for a free topo I molecule was found to be higher than 0.5 (Figure 7b).

However, the Trp bands around 880 cm^{-1}, sensitive to the strength of H-bonds formed by the NH group, are found in the Raman spectrum at two positions, 868 and 883 cm^{-1}, with about 1:1 relative intensity. The former band is characteristic of very strong H-bonding, while the latter presumes the fraction of Trp residues that are free from H-bonding (*26*). Assuming similar Raman cross sections for the 880 cm^{-1} band in both states of Trp, 6−7 of the 13 Trp should be non-H-bonded. Since no band at 877 cm^{-1} corresponding to H-bonding to water molecules is detected, we conclude that all the Trp residues are inaccessible to solvent. This is consistent with the intense 1358 cm^{-1} band, which implies a largely hydrophobic environment for the Trp residues.

On interaction with the solig, the I_{1358}/I_{1345} intensity ratio (an indicator of Trp hydrophobicity) increases to 1.0, which implies even more Trp residues are involved in hydrophobic interactions. The ca. 880 cm^{-1} band of Trp (sensitive to the strength of H-bonds of the NH group) is still found in the differential Raman spectrum (68-kDa topo I/solig spectrum minus solig spectrum) in the same position as that for the free 68-kDa topo I—883 cm^{-1}. So, analysis of this band shows that some Trp residues of the topo I should conserve the bonding state of the NH group when in complex with the solig. Unfortunately, we failed to distinguish strongly H-bonded Trp residues (characterized by the 868 cm^{-1}

Raman band) due to overlapping with the solig's bands in this region (Figure 4).

Another indole ring vibration (at ca. 1550 cm^{-1}) changes in frequency as a function of torsional angle C2−C3−Cβ−Cα($\chi^{2,1}$), defining the orientation of the indole ring of Trp with respect to the Cα atom of the amino acid backbone (*27*). The range of frequency variation (1540−1560 cm^{-1}) is large enough to determine the torsional angle in the 60−120° range from the Raman spectra. Three subsets of Trp bands are revealed in this region of the spectrum of the 68-kDa topo I, 1545, 1550 and 1560 cm^{-1}. These, respectively, correspond to the values of $\chi^{2,1}$ of 80°, 95°, and 120° (Figure 7d). By normalization the intensities of the 1545, 1550, and 1560 cm^{-1} bands to the total integral intensity, 6−7 of the 13 Trp residues are concluded to have $\chi^{2,1}$ equal to ca. 95°; the 3−4 Trp should adopt ca. 80°, and another 3−4 molecules must take ca. 120°. Remarkably, the Raman spectrum of Trp in an aqueous buffer reveals the band at 1553 cm^{-1} giving a $\chi^{2,1}$ value of ca. 100° (*33*). Thus, about 6−7 Trp residues (49%) adopt an orientation of the indole ring very close to a "free" Trp in aqueous buffer solution, and therefore, these molecules are very likely to be those free from H-bonding Trp residues (giving rise to the band at 883 cm^{-1}). On the other hand, the remaining 6−7 Trp residues (one-half of which have ca. 80° and the other half exhibit $\chi^{2,1} = 120°$) are those whose orientation is changed from the nonbound state in free 68-kDa topo I to a strongly H-bonded state upon complex formation, and these residues evidently contribute to the band at 868 cm^{-1}.

Three subsets of Trp bands are revealed in this region in the differential Raman spectrum (68-kDa topo I/solig spectrum minus solig spectrum) viz. 1540, 1545, and 1555 cm^{-1}, corresponding to the $\chi^{2,1}$ values of 60°, 80°, and 100°, respectively (Figure 7c). By normalization of these intensities to the total integral intensity of bands within this region, 44% of the 13 Trp are concluded to have $\chi^{2,1}$ angles equal to ca. 100°; the 33% should take ca. 60°, and the 23% should adopt ca. 80°. Thus, 25% of the "free"-oriented Trp of a 68-kDa topo I molecule is conserved upon enzyme/solig complex formation. Again, another 25% of the ca. 80°-oriented Trp is still found in 68-kDa topo I bound to solig. On the other hand, about four of the remaining Trp residues adopt new orientation of the indole ring, different from that of 68-kDa topo I in solution, with a $\chi^{2,1}$ value of ca. 60°. Such reorientation must indicate the occurrence of specific, solig-induced interactions of the Trp residues that are different from those found for the 68-kDa topo I in solution.

Protein Secondary Structure Probed by Raman and CD Spectroscopy. (a) 68-kDa Topo I. The spectrum shown in Figure 4d contains the amide I and amide III bands centered at 1646 and 1251 cm^{-1}, respectively, which indicate that the predominant secondary structure of the protein is α-helix. The $C_\alpha-C_\beta$ stretching vibration at 937 cm^{-1}, which is diagnostic of side chains incorporated into α-helical domains (*23*), is extremely intense in the Raman spectrum of the 68-kDa topo I. Deconvolution of the main amide I and III bands reveals shoulders related to additional β-conformation (1679 cm^{-1} for amide I and 1241 cm^{-1} for amide III) and irregular (1668 cm^{-1}) domains. On the basis of analysis of the Raman amide I band with the RIP technique, we conclude that the 68-kDa topo I contains 58.5% α-helix, 24.4% β−sheet, and 17.1% other structures (Table 1).

Table 1: Composition of the Global Contents of Secondary Structure of the Recombinant Human 68-kDa topo I in Solution Free and in Complex with Suicide Oligonucleotide (Underlined)

	experimental				theoretical prediction
structure type	Raman		CD		LINK
α-helix (%)	58.5	44.7	44	29	58.5
β-sheet (%)	24.4	29.3	31	40	24.7
other structures (%)	17.1	26.0	25	31	16.8

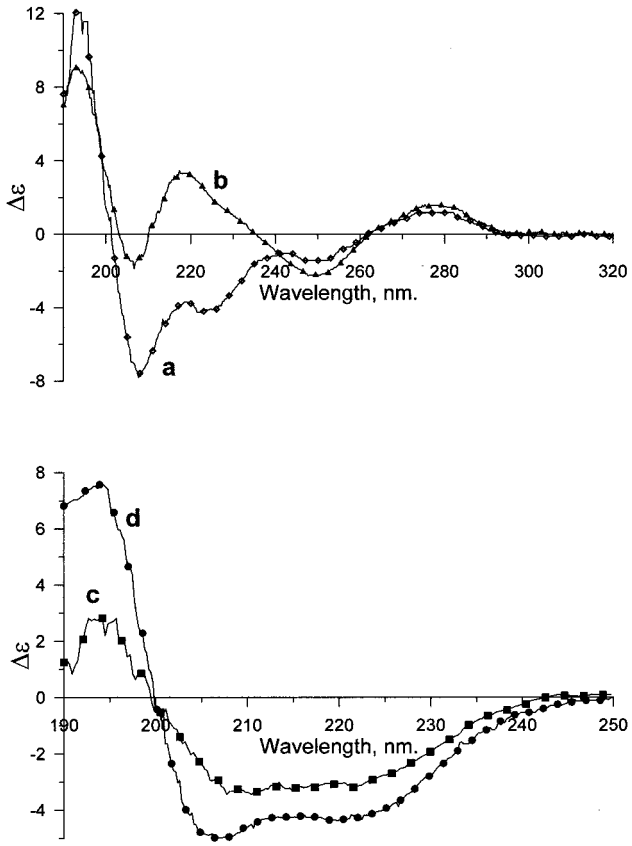

FIGURE 8: CD spectra of 68-kDa topo I/solig complex (a), pure solig (b) in the region 190−320 nm, topo I/solig complex with subtracted signal of solig (c), and pure 68-kDa topo I (d) in the region 185−250 nm. Protein concentration is 9 mg/mL. Optical length of the cell is 0.001 cm.

The content of the α-helix obtained for the 68-kDa topo I from Raman data is remarkably higher than that reported recently for a 70-kDa recombinant topo I fragment missing the first 174 N-terminal amino acids (*4*). The molecular mass of the α-helix for a 70-kDa recombinant topo I was calculated from CD spectra to be 28 kDa (40%). The CD spectrum of the 68-kDa topo I (Figure 8d) recorded in our work under the same conditions as those used for the Raman spectrum shows similar molar ellipticity values as those observed for the CD spectrum presented by Stewart et al. in the ca. 190−210 nm region (*4*). The α-helix content estimated from the CD spectrum of the 68-kDa topo I gives 44% α-helix (Table 1), which is not too far from the value reported by Stewart et al. (*4*). The calculation of protein conformation from CD data systematically underestimates the percentage of α-helix and overestimates those of β-sheet and other structures as compared with the RIP method based on the Raman data (Table 1). It is in general agreement with reports indicating that the calculations of the helix structure from CD spectra often assign a significant part of

mono-α-helix to "undefined conformation" (*17*, *42*). This normally results an underestimation of the helical content in predominantly α-helical proteins. This is kept in mind hereafter when comparing the CD and Raman data on the 68-kDa topo I conformation.

(b) 68-kDa Topo I in Complex with Suicide Oligonucleotide. The spectrum shown in Figure 4c contains the amide I and amide III bands centered at 1667 and 1249 cm^{-1}, respectively. Deconvoluted main amide I and III bands yield shoulders, indicating additional β-conformation (1682 cm^{-1} for amide I and 1241 cm^{-1} for amide III) and irregular (1671 cm^{-1}) domains. On the basis of analysis of the Raman amide I band with the RIP technique, it was calculated that the 68-kDa topo I fragment, when in complex with the solig, contains 45% α-helix, 29% β-sheet, and 26% other structures (Table 1).

The CD spectra of the 68-kDa topo I/solig complex and the 68-kDa topo I alone obtained after subtraction of the spectrum of the solig (Figure 8b) are shown in Figure 8 parts a and c. The conformation of the bound 68-kDa topo I calculated from the CD spectrum gives the values of 29% α-helix, 40% β-sheet, and 31% other structures (Table 1).

By comparison of conformation data for the free and bound protein, it can be concluded that despite the discrepancies in determination of the absolute contents of the secondary structures with CD and Raman methods, the relative changes in the 68-kDa topo I secondary structure induced by complexation with the solig are very similar: 14% (Raman) and 15% (CD) decrease of α-helix, 5% (Raman) and 9% (CD) increase of β-sheet, 9% (Raman) and 6% (CD) increase of other structures.

Structural Model of 68-kDa Topo I from Statistical Prediction Techniques. The application of the standard statistical algorithms of protein structure prediction usually reveals several "questionable" segments, which can form various secondary structures. To identify such conformationally labile segments in the 68-kDa topo I, the results of local secondary structure distributions obtained from the Chou−Fasman methods and Garnier algorithms (*10*, *21*, *22*), with lower cutoff values for the mean conformational parameters of α-helix and β-sheet, were analyzed (Table 1).

For labile segments, the mean conformational parameters of different types of regular structure are very similar. Therefore, a number of additional factors (e.g., distribution pattern of hydrophobic and charged residues, secondary structure of adjacent segments in βαβ Rossman folds, presence of β-turn, disulfide bond formation) must be taken into account. We used the methods of LINK (*10*, *11*) in which the Raman spectroscopy data or X-ray structure results (*5*, *6*) are combined with prediction techniques. It procured additional experimental information, which enables empirically predicted regions of the local secondary structure to be adjusted along the polypeptide chain of the 68-kDa topo I. As soon as such an adjustment was completed, the statistical predictions of secondary structure reproduced exactly the RIP method data (Table 1) and the model of the conformation of 68-kDa topo I was proposed (see Discussion).

DISCUSSION

Recombinant 68-kDa human DNA topo I (residues 191−765) expressed, purified, and characterized in this work exhibits practically the same specific cleavage and relaxation activities as the full-length protein (Figures 1−3). Developed here, the FLD assay for monitoring of the real-time sc DNA relaxation by 68-kDa topo I shows also that this reaction is inhibited by CPT at concentrations similar to those that inhibit the intact enzyme (Figure 3). The further advantages of the FLD approach include the possibility of quantitative analysis of the form of the relaxation curves, which should reflect the details of the catalytic mechanism of enzyme inhibition with the different drugs (*12*).

Very recently, the crystal structures of "reconstituted" human topo I (obtained by mixing the purified 58-kDa core domain and the 6.3-kDa C-terminal domain) in covalent and noncovalent complexes (*5*) and of 70-kDa N-terminally truncated human topo I nonactive mutant in noncovalent complex with 22-bp DNA duplexes (*6*) have been solved, and a model for the mechanism of human topo I has been proposed (*6*). It should be noted that these successful structural studies were restricted to the topo I/DNA complexes; the crystals of the free enzyme were not obtained, there is no information concerning the structure of free topo I, and direct comparison of the topo I structure with that within the complexes with DNA is not available now.

In this paper, we have used Raman and CD spectroscopic techniques to analyze the 68-kDa topo I conformational transformations in solution induced by suicide covalent complex formation and have applied the combined spectroscopic−theoretical (LINK) approach to localize the protein domains exhibiting a significant potential for solig-induced 68-kDa topo I structural transformation. Both Raman and CD spectroscopy proved to be effective techniques for studies of the protein secondary structure variations, yet Raman spectroscopy is also extremely sensitive to detection of variations in geometry and microenvironment of the side chains of individual amino acid residues (*13*, *23*).

Spectroscopic techniques were used to study the mechanistical aspects of the DNA binding and cleavage 68-kDa topo I half-reaction by decoupling these steps of the topo I catalytic cycle from the others using topo I solig-substrate. The solig used in this work corresponds to the group of sites, occurring repetitively in the rDNA spacers of *Tetrahymena* (*45*) and *Dictyostelium* (*46*) and cleaved with high efficiency by the topo I from all species tested (*47*). Thus, these sequences function as highly active catalytic sites for DNA relaxation (*48*). A single cloned site of this type has been used to investigate binding properties of the topo I (*43*). It was shown that the topo I stabilizes the DNA duplex on the upstream side from the solig cleavage site, while the duplex on the downstream side from the cleavage site is relatively unaffected by the binding of the enzyme. The weak binding of the topo I to sequences downstream from the solig cleavage site was characterized by high rates of suicide cleavage, e.g., cleavage without concomitant religation of minimal DNA substrates to this side. It was also shown that CPT does not affect the cleavage reaction of topo I at this model DNA site, while the religation reaction is inhibited to a sufficient extent (*2*).

Our work addresses the following questions: (i) determination of the free 68-kDa human topo I secondary structures content with the spectroscopic techniques and characterization of microenvironment of individual amino acid residues (Tyr, Trp, Cys) of the enzyme in solution and construction

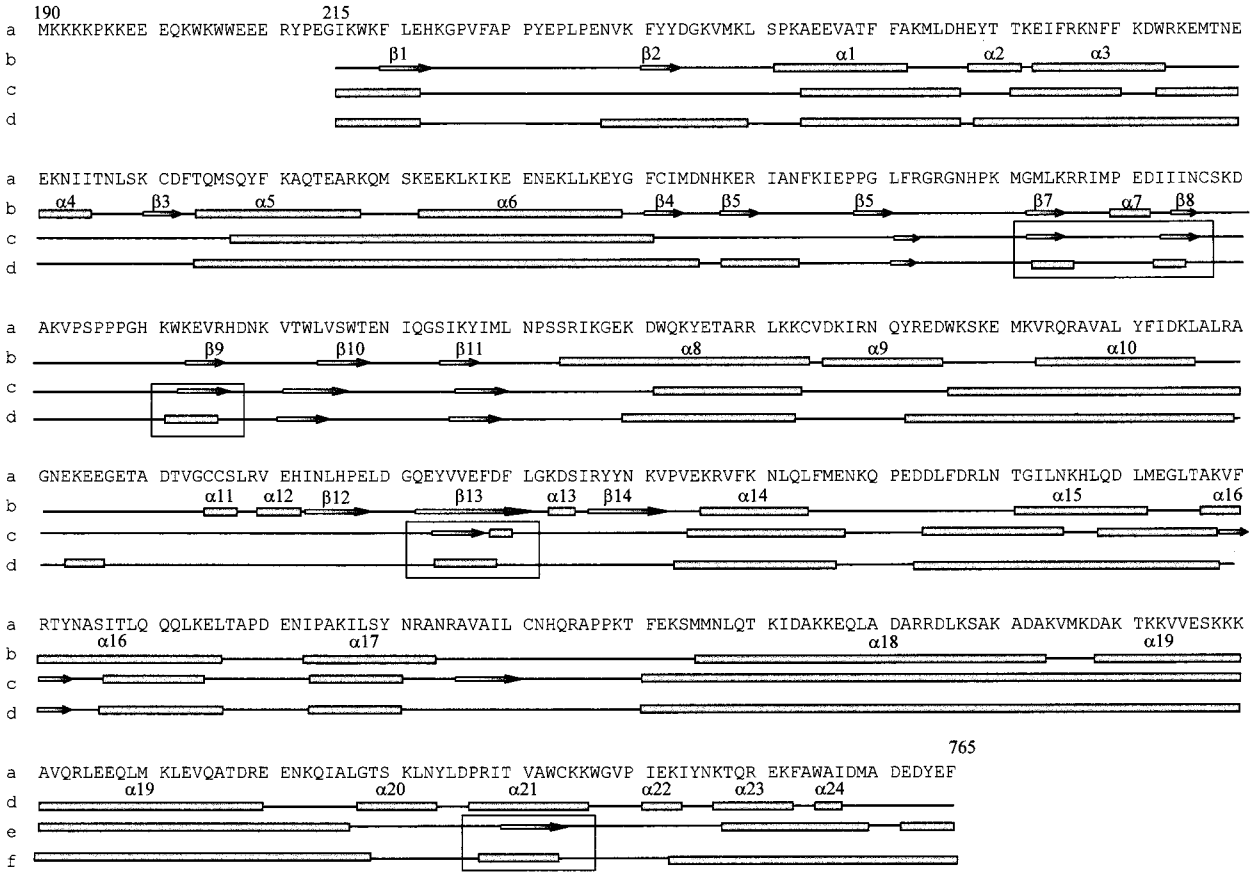

FIGURE 9: (a) 68-kDa human topoisomerase I primary structure. (b) 68-kDa topoisomerase I secondary structure distribution along the protein primary structure derived from the crystal structure of topoisomerase I/DNA complex solved in refs *5* and *6*. (c) The same as in (b), obtained with the LINK method (see text for details). (d) The same as in (b) obtained with the LINK method for free 68-kDa topoisomerase I in solution. The regions of the β-structure are indicated with arrows and of the α-helix with cylinders. The topoisomerase I sequences exhibiting high potential for the secondary structure transitions induced by the DNA binding and cleavage are included in the parallelepipeds.

of the model of 68-kDa topo I secondary structures distribution along the protein primary structure using the LINK technique and (ii) spectroscopic identification of the 68-kDa topo I conformational transitions in solution induced by solig binding and cleavage and localization of the most probable protein segments with the potential of solig-induced conformational transition.

The total percentage of α-helix for the DNA-bound protein calculated from the Raman spectra in solution (44.7%, Table 1) is found to be practically the same as that in the crystal (47%; see ref *5*). On the other hand, the percentage of the β-sheets obtained from the X-ray analysis (10.5%) is quite different from the percentage of β-structure and β-sheets calculated from the Raman spectra (29.3%). This is not surprising because Raman spectroscopy (and other spectroscopic techniques) attributes to the β-structure even the very short (two to three residues) protein segments or even the individual amino acid residues exhibiting the geometrical characteristics similar to those for the residues within the longer β-sheets (*17*, *18*). These short segments and individual amino acid residues are normally attributing to "unordered structures" in X-ray analysis.

The results of our spectroscopic measurements provide direct evidence of the conformational transition of the enzyme induced by solig binding and cleavage in solution. Both Raman and CD spectral calculations demonstrated that nearly 15% of the α-helix of 68-kDa topo I (ca. 80 peptide groups of the protein) are transferred within the other structures upon complexation and cleavage of the solig. So, the free 68-kDa human topo I was found to include ca. 58.5% (instead of 44.7% for topo I/solig complex) α-helix in solution (Table 1).

Combination of the experimental data with the statistical methods of the LINK technique enables us to propose the model of protein secondary structure distribution along the primary sequence. Taking into account overestimation of the percentage of β-structure by Raman spectroscopy compared with the X-ray data and in order to evaluate the potency of LINK technique, we have used the total percentages of α-helix and β-sheets calculated from the X-ray data (*5*) for statistical predictions made by the LINK. Figure 9 parts b and c presents direct comparison of the secondary structure of the enzyme within the topo I/DNA complex in crystal (*5*, *6*) with that obtained with the LINK technique. There are only 20 residues within the 68-kDa topo I (ca. 4%) for which the LINK technique predicted differently from the X-ray (α-structure instead of the β-structure or vice versa) secondary structure. So, the LINK technique obviously shows its potential in adequate prediction of secondary structure distribution along the 68-kDa topo I primary structure and, therefore, may be applied for identification of the regions with a significant potential of modification in the result of protein/DNA interactions.

Experimental results of Raman and CD spectroscopies in solution demonstrated that ca. 15% of topo I secondary structures are transformed upon complexation with the DNA

substrate (Table 1). Using these data, we calculated the secondary structure distribution of the free 68-kDa topo I along the protein primary structure (Figure 9d). Comparison of Figure 9 parts c and d shows that the significant domains of the 68-kDa topo I are not demonstrating any potential of the secondary structure transitions in the result of topo I/DNA binding (α1−α4, α5−α6, *β*6, *β*10−*β*11, α8, α14, α18−α20, α23−α24). These domains are separated with the much smaller regions exhibiting high potential of the α → *β* transformations (*β*7−α7 − *β*8−*β*9; *β*13, α21; the region between α14 and α15). One may suppose that these labile regions may change their secondary structure due to the DNA-induced relative motion of the protein structural domains.

The 68-kDa topo I protein secondary structure transformations (ca. 80 peptide groups per molecule of 68-kDa topo I) in solution were found to be accompanied by changes in geometry of disulfide bonds and so probably involve relative movement of the protein structural domains. Spectroscopy data in solution show also that the binding and cleavage of the solig changes the system of H-bonds formed by the Tyr residues. Six of the 19 Tyr residues of the 68-kDa topo I change the type of their H-bonding. Moreover, the microenvironment and geometry of side chains of 4 of the 13 Trp residues were changed for the 68-kDa topo I/solig complex, when compared with the free 68-kDa topo I.

How does topo I manipulate the DNA strands? It is now well-established that the basic covalent chemistry involves two successive transesterification reactions. In the first reaction, an enzyme tyrosyl group attacks an internucleotide phosphorus, forming a tyrosine−phosphate linkage at one end of the transiently broken DNA strand and leaving a hydroxyl group on the deoxyribose at the other end of the broken strand. The second reaction reverses the first, resulting in rejoining of the DNA strand and setting the enzyme free from covalent attachment to DNA. The two reactions are separated temporally by the transport of the DNA strand through the DNA gate. One reaction is likely to be the exact microscopic reversal of another, but different amino acid groups of an enzyme could in principle participate in the two reactions (*1*, *7*).

The most intriguing mechanistic aspects of DNA topos I are the steps by which they move DNA strands one through another. For the type I-5′ subfamily of topo I (bacterial (*E. coli*) DNA topo I, reverse gyrase, etc.) cleaving single DNA strands and forming a 5′-phosphotyrosine covalent intermediate, the combined biochemical and structural results strongly favor the "enzyme-bridging" model of DNA strand passage (ref *1* and references therein). In this model, the enzyme holds onto both ends of the transiently severed DNA strand, and the enzyme-bound DNA ends are moved apart enough to allow the passage of another DNA strand. For the type I-3′ subfamily of enzymes (eukaryotic, *vaccinia virus*, etc.) binding duplex DNA, cleaving one of the strands, and forming a 3′-phosphotyrosine covalent intermediate, whether the enzyme-bridging model also applies is less certain. In the alternative DNA rotation model, the enzyme/DNA interaction is assumed to involve mainly DNA on the scissile strand that becomes covalently linked to the enzyme in the first transesterification reaction; the enzyme has only a passive role in DNA strand passage, which occurs by rotation of the DNA segments on the two sides of the enzyme-linked DNA phosphoryl group relative to each other. Although there is some indication of interaction between eukaryotic topo I and DNA downstream of the site of DNA breakage (*43*), a similar interaction between DNA and *vaccinia virus* topo I has not been observed (*44*). In the limiting cases, the enzyme-bridging model requires the removal of only one supercoil per DNA cleavage−religation cycle, whereas in the DNA-rotation model, all supercoils can be removed by as few as one single DNA breakage−rejoining cycle. Other than the limiting cases, however, the distinction between the two models is not clear-cut, as interaction between the enzyme and DNA downstream of the scissile bond may range from very weak to very strong.

The DNA-rotation and enzyme-bridging models represent the two extremes of a continuum in the conceptual framework for how topo I might effect changes in the linking number (*6*). From the general point of view, the enzyme-bridging model should require massive structural transformation of topo I, whereas the passive role of the enzyme in DNA strand passage in the frames of the DNA-rotation model does not require it (refs *1* and *7* and references therein). The structures of human topo I/DNA covalent and noncovalent complexes presented in refs *5* and *6* assume that relaxation occurs by an intermediate mechanism called controlled rotation, in which ionic interactions between the DNA, the nose cone helices, and the linker domain regulate the winding process.

Our spectroscopic data for topo I and topo I/DNA complex in solution present the first direct experimental evidence of a topo I protein conformational step after the cleavage step in the forward human topo I cleavage reaction. As a basis for the crystal structures of topo I/DNA complexes, Stewart et al. (*6*) proposed that the free enzyme initially exists in a "open" conformation, which is most likely achieved by a hinge-bending motion located at the interface between core subdomains I and III and the boundary between two helices including the residues 434−453 and 455−464, respectively. It was also proposed that the binding event is directed in large part by the surface and charge complementarity of the enzyme and DNA and culminates in the complete embrace of the DNA. These movements of charged surfaces should certainly change the microenvironment of the residues with the potency of formation of H-bonds, and this effect should be detected by Raman spectroscopy in solution. DNA-induced "closing" of the enzyme due to relative rotation of the protein structural domains (*6*) is supported also by the limited proteolysis data (some regions of the protein that are sensitive to proteolysis in the absence of DNA become resistant upon DNA binding (*3*)) and may be responsible for the changes of hydrophobicity of Trp(s) microenvironment detected by Raman spectroscopy in solution.

The pattern of redistribution of protein secondary structures induced by solig binding and covalent suicide complex formation (Figure 9) supports the model of intramolecular bipartite mode of topo I/DNA interaction in solution in the cleavage reaction. Under this model, topo I mediated DNA cleavage requires enzyme interaction with two distinct DNA duplex regions located around the cleavage site and on the side holding the 5′-OH end generated by DNA cleavage (*49*). We propose that the solig-induced protein secondary structure transformations within the two distinct 68-kDa topo I core and C-terminal domains (Figure 9) may be provoked by the

interactions of the core and C-terminal domains of the topo I with the two distinct DNA duplex regions located around the cleavage site.

The next step of our work includes Raman, CD, and FLD structural analysis of the pH and ionic strength dependence of the 68-kDa topo I catalytic reactions in solution. Our further work includes also analysis of the ternary complexes formed by 68-kDa human topo I, plasmid DNA, and CPT derivatives.

REFERENCES

1. Wang, J. C. (1996) *Annu. Rev. Biochem. 65*, 635−692.
2. Svejstrup, J. Q., Christiansen, K., Gromova, I. I., Andersen, A. H., and Westergaard, O. (1991) *J. Mol. Biol. 222*, 669−678.
3. Stewart, L., Ireton, G. C., and Champoux, J. J. (1996) *J. Biol. Chem. 271*, 7602−7608.
4. Stewart, L., Ireton, G. C., Parker, L. H., Madden, K. R., and Champoux, J. J. (1996) *J. Biol. Chem. 271*, 7593−7601.
5. Redinbo, M. R., Stewart, L., Kuhn, P., Champoux, J. J., and Hol, W. G. J. (1998) *Science 279*, 1504−1513.
6. Stewart, L., Redinbo, M. R., Qiu, X., Hol, W. G. J., and Champoux, J. J. (1998) *Science 279*, 1534−1541.
7. Gupta, M., Fujimori, A., and Pommier, Y. (1995) *Biochim. Biophys. Acta 1262*, 1−14.
8. Nunes-Dyby, S. E., Matsumoto, L., and Landy, A. (1987) *Cell 50*, 779−788.
9. Doolitle, R. F., Ed. (1996) *Methods Enzymol. 266*, 1−680.
10. Alix, A. J. P. (1997) in *Biomolecular Structure and Dynamics: Recent experimental and theoretical advances, NATO, Advanced Studies Institute* (Vergoten, G., and Theophanides, Eds.), series E, Applied Science, Vol. 342, pp 121−150, Kluwer Academic Publishers, Dordrecht.
11. Alix, A. J. P., Goulyaev, D. I., and Efremov, R. G. (1995) in *Spectroscopy of biological molecules* (Merlin, J. C., Turrell, S., and Huvenne, J. P., Eds.) pp 89−90, Kluwer Academic Publishers, Dordrecht.
12. Gololobov, G., Chernova, E., Schourov, D., Smirnov, I., Kudelina, I., and Gabibov, A. (1995) *Proc. Natl. Acad. Sci. U.S.A. 92*, 254−257.
13. Thomas, G. J., Jr. (1987) in *Biological Applications of Raman Spectroscopy Vol. 1*, (Spiro, T. G., Ed.), *Raman Spectra and the Conformations of Biological Macromolecules* pp 135−201, Wiley-Interscience, New York.
14. Provencher, S. W. (1982) *Technical Report EMBL DAO5*, Heidelberg.
15. Berjot, M., Marx, J., and Alix, A. J. P. (1987) *J. Raman Spectrosc. 18*, 289−300.
16. Debelle, L., Alix, A. J. P., Jacob, M.-P., Huvenne, J.-P., Berjot, M., Sombret, B., and Legrand, P. (1995) *J. Biol. Chem. 270*, 26099−26103.
17. Ovchinnikov, Yu. A., Arystarkhova, E. A., Arzamazova, N. M., Dzhandzhugazyan, K. N., Efremov, R. G., Nabiev, I. R., and Modyanov, N. N. (1988) *FEBS Lett. 227*, 235−239.
18. Pourplanche, C., Lambert, C., Berjot, M., Marx, J., Chopard, C., Alix, A. J. P., and Larreta-Garde, V. (1994) *J. Biol. Chem. 269*, 31585−31591.
19. Haaland, D. M., and Thomas, E. V. (1988) *Anal. Chem. 60*, 1202−1206.
20. Sun, J. (1995) *J. Chemom. 9*, 21−25.
21. Prevelige, P., and Fasman, G. D. (1989) in *Prediction of protein structure and the principles of protein conformation* (Fasman, G. D., Ed.) pp 391−416, Plenum Press, New York and London.
22. Garnier, J., and Robson, B. (1989) in *Prediction of protein structure and the principles of protein conformation* (Fasman, G. D., Ed.) pp 417−465, Plenum Press, New York and London.
23. Spiro, T. G., Ed. (1987) *Biological Applications of Raman Spectroscopy, Vol. 1, Raman Spectra and the Conformations of Biological Macromolecules* Wiley-Interscience, NY.
24. Siamwiza, M. N., Lord, R. C., Chen, M. C., Takamatsu, T., Harada, I., Matsuura, H., and Shimanouchi, T. (1975) *Biochemistry 14*, 4870−4876.
25. Harada, I., Takeuchi, H. (1986) in *Advances in Spectroscopy Vol. 13, Spectroscopy of Biological Systems* (Clark, R. J. H., Hester R. E., Eds.), Chapter 3, p 116, Wiley, Chichester.
26. Miura, T., Takeuchi, H., and Harada, I. (1988) *Biochemistry 27*, 88−94.
27. Miura, T., Takeuchi, H., and Harada, I. (1989) *J. Raman Spectrosc. 20*, 667−671.
28. Li, H., and Thomas, G. J., Jr. (1991) *J. Am. Chem. Soc. 113*, 456−462.
29. Li, T., Chen, Z., Johnson, J. E., and Thomas, G. J., Jr. (1992) *Biochemistry 31*, 6673−6682.
30. Benevides, J. M., and Thomas, G. J., Jr. (1983) *Nucleic Acids Res. 11*, 5747−5761.
31. Erfurth, S. C., and Peticolas, W. L. (1975) *Biopolymers 14*, 247−256.
32. Benevides, J. M., Wang, A. H.-J., van der Marel, G. A., van Boom, J. H., Rich, A., and Thomas, G. J., Jr. (1984) *Nucleic Acids Res. 12*, 5913−5925.
33. Bare, G. H., Alben, J. O., and Bromberg, P. A. (1975) *Biochemistry 14*, 1578−1588.
34. Alben, J. P., Bare, G. H., and Bromberg, P. A. (1974) *Nature (London) 252*, 736−739.
35. Sugeta, H., Go, A., and Miyazawa, T. (1972) *Chem. Lett.* 83−89.
36. Sugeta, H., Go, A., and Miyazawa, T. (1973) *Bull. Chem. Soc. Jpn. 46*, 3407−3409.
37. Van Wart, H. E., and Sheraga, H. A. (1976) *J. Phys. Chem. 80*, 1812−1822.
38. Van Wart, H. E., and Sheraga, H. A. (1976) *J. Phys. Chem. 80*, 1823−1829.
39. Vorotyntseva, T. I., Surin, A. M., Trakhanov, S. D., Nabiev, I., and Antonov, V. K. (1981) *Biorg. Khim. 7*, 45−59.
40. Stivers, J. T., Shuman, S., and Mildvan, A. S. (1994) *Biochemistry 33*, 327−339.
41. Thomas, G. J., Jr., Prescott, B., and Day, L. A. (1983) *J. Mol. Biol. 165*, 321−356.
42. Williams, R. W., McIntyre, J. O., Gaber, B. P., and Fleischer, S. (1986) *J. Biol. Chem. 261*, 14520−14524.
43. Stevsner, T., Mortensen, U. H., Westergaard, O., and Bonven, B. J. (1989) *J. Biol. Chem. 264*, 10110−10113.
44. Sekiguchi, J., and Shuman, S. (1994) *J. Biol. Chem. 269*, 29760−29764.
45. Bonven, B. J., Gocke, E., and Westergaard, O. (1985) *Cell 41*, 541−551.
46. Ness, P. J., Koller, T., and Thoma, F. (1988) *J. Mol. Biol. 200*, 127−139.
47. Christiansen, K., Bonven, B. J., and Westergaard, O. (1987) *J. Mol. Biol. 193*, 517−525.
48. Busk, H., Thomsen, B., Bonven, B. J., Kjeldsen, E., Nielsen, O. F., and Westergaard, O. (1987) *Nature 327*, 638−640.
49. Christiansen, K., and Westergaard, O. (1994) *J. Biol. Chem.* 269, 721−729.

BI9806495